

Laser Pulse Timing Detector

Tarmo Ruotsalainen, Pasi Palojärvi, Tero Peltola, Juha Kostamovaara

University of Oulu, Dept. of Electrical Engineering, Electronics lab.
Linnanmaa, SF-90570 Oulu, Finland
tel: +358-81-553 2685, fax: +358-81-553 2700, email: tarmo@ee.oulu.fi

***Abstract.** A laser pulse timing detector has been designed. The circuit consists of a low-noise transimpedance amplifier channel with gain control and a timing detector. The measured bandwidth of the amplifier channel is 10 MHz, transimpedance 340 k Ω - 2.7 M Ω and input referred noise 0.9 pA/ $\sqrt{\text{Hz}}$. The walk error of the timing detector is +/- 50 ps, when its input signal amplitude varies from 150 mV to 2.5 V.*

1. Introduction

The goal of this work is to develop an integrated laser pulse detector with high sensitivity for a distance measurement application. In this application laser pulses with a width of ~ 40 ns are used, so a bandwidth of ~ 10 MHz is needed. The main objectives are the minimization of the noise of the preamplifier to maximize the measurement range and to optimize the timing detection accuracy.

2. Construction

The detector designed here is shown in Fig. 1. The received laser pulses are detected with a photodiode and amplified in the transimpedance amplifier channel to a level which is suitable for timing detection. The timing detector produces accurately timed logic level output pulses for a time interval measurement circuitry. A noise comparator is used to enable the timing comparator only when the amplitude of the input pulses is higher than a preset threshold value in order to prevent the noise from causing false detections. The output of the rms meter can be used to adjust the threshold value, which is important in a noisy environment.

The whole receiver channel is differential to reduce disturbances and the sensitivity to them. Furthermore, all the blocks have their own separate power supplies and local substrate contacts.

The main factors limiting the accuracy of the timing detection are noise, which causes random variation in the timing point, and amplitude variation, which affects the delay of the timing comparator.

3. Noise Optimization

The transimpedance preamplifier is composed of the voltage amplifier shown in Fig. 2 and feedback resistors. The dominant noise sources of the amplifier channel are the feedback resistors and the bipolar input transistors of the preamplifier, as shown in Fig. 3. The noise performance is optimized by minimizing both the noise sources and their transfer functions to the output. The noise voltage at the output of the preamplifier is (see Fig. 3):

$$u_{no}^2 = \frac{4kTR_f}{1 + \left(\omega C_{TA(f)} \frac{R_f}{R_f}\right)^2} + \frac{1 + (\omega C_{TR_f})^2}{1 + \left(\omega C_{TA(f)} \frac{R_f}{R_f}\right)^2} \cdot u_{nT}^2 + \frac{R_f^2}{1 + \left(\omega C_{TA(f)} \frac{R_f}{R_f}\right)^2} \cdot i_{nT}^2 \quad (1)$$

Large feedback resistors R_f with a value of 100 k Ω are used to minimize their thermal noise. Wide input transistors with low bias currents are used to minimize the thermal noise of the base resistance (u_{nT}), the shot noise of the base current and the shot noise of the collector current (i_{nT}).

The photodetector used in the application is relatively large, $C_d \sim 2$ pF, and the parasitic capacitances of the package and the PCB are several picofarads, so the total capacitance C_T is ~ 5 pF. It is seen in (1) that this capacitance boosts the effect of u_{nT} at higher frequencies. To overcome this effect the noise bandwidth is limited with 5 poles: 3 poles in the preamplifier and 2 poles in the post amplifier. The internal voltage amplifier of the preamplifier has 2 poles and 1 pole is formed in the input of the preamplifier, so the high frequency noise is very effectively filtered in the preamplifier. The gain and the frequency of the 2 internal poles of the voltage amplifier were carefully designed to ensure the stability of the feedback loop.

In this case, according to simulations the differential structure was found to have a noise performance comparable to a similar single-ended one. The disadvantage of the more complex differential structure is partly compensated by the fact that the common mode parasitic capacitances in the input node have less effect in the differential preamplifier (C_T is smaller) and thus the noise contribution of the voltage noise u_{nT} is reduced.

4. Timing Detection

The timing point should be independent of the amplitude of the input pulses. This is achieved by “integrating” and “differentiating” the input pulses with RC-sections as shown in Fig. 4 and detecting the crossing of the output signals with a fast comparator. As the highpass and lowpass filters are linear, the shape of their output pulses is independent of the signal amplitude. The delay of a comparator is a function of the input signal slew rate SR_{inp} and underdrive/overdrive, the delay being shortest with large pulses with fast edges. Using a simple

approximation the delay t_{dcomp} of a comparator is [1]:

$$t_{dcomp} \approx t_{dmin} + \frac{B}{\sqrt{SR_{inp}}}, \quad (2)$$

where t_{dmin} is the minimum delay and B is a constant depending on the bandwidth of the comparator. This delay variation can be partly compensated by arranging smaller signals to cross earlier in the input of the timing comparator. This can be accomplished by adding a small offset voltage with right polarity to the input signal as shown in Fig. 5. Using a linear approximation the effect of the offset voltage U_{off} on the timing detection result is:

$$w_{det} \approx -\frac{U_{off}}{SR_{inp}} \quad (3)$$

Combining (2) and (3) gives the total walk error w_{tot} :

$$w_{tot} \approx w_{comp} + w_{det} \approx \frac{B}{\sqrt{SR_{inp}}} - \frac{U_{off}}{SR_{inp}} \quad (4)$$

The walk error cannot be totally eliminated with this scheme, because the dependencies of the terms of (4) on SR_{inp} are not the same, but the error can be minimized in the useful operating region as shown in Fig. 5. With smaller signals, when the compensation is poor, noise prevents the use of the detector in any case. A high/lowpass corner frequency of 2 MHz was found to give the smallest walk error and best single shot resolution in this particular case.

5. Measurement results

The input referred current noise of the amplifier channel was measured to be $0.9 \text{ pA}/\sqrt{\text{Hz}}$ (total output noise voltage divided by the transimpedance and the square root of the signal bandwidth) and the input dynamic range 2800. The temperature and supply voltage sensitivities of the delay of the receiver channel were $100 \text{ ps}/^\circ\text{C}$ and $1.25 \text{ ns}/\text{V}$, respectively. Since two identical channels are used in the application (one for the start and one for the stop mark of the time interval), only the matching of the sensitivities is important, not their absolute value.

The variation of the timing detection result as a function of the input signal amplitude of the timing detector is shown in Fig. 6. The distance measurement result varies about $\pm 50 \text{ ps}$, when the input amplitude varies from 150 mV to 2.5 V . The single shot resolution of the detection is shown in Fig. 7 and is 200 ps with good SNR. The timing error caused by the R-2R attenuator is $\pm 125 \text{ ps}$, when the gain is changed from min. to max. The circuit was fabricated in the AMS $1.2 \mu\text{m}$ BiCMOS process.

6. Conclusions

Measurement results show that a dm-level distance measurement accuracy has been achieved. By minimizing both the noise sources and their transfer functions to the output a noise level of

0.9 pA/ \sqrt{Hz} has been reached. The delay variation of the timing comparator can be effectively compensated with a small offset voltage.

References

1. Arbel A.F. (1980) Analog Signal Processing and Instrumentation. Cambridge University Press, J. W. Arrowsmith Ltd., Bristol, England.

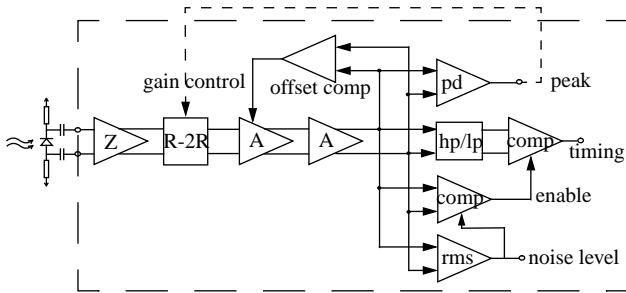


Fig. 1. BiCMOS receiver channel.

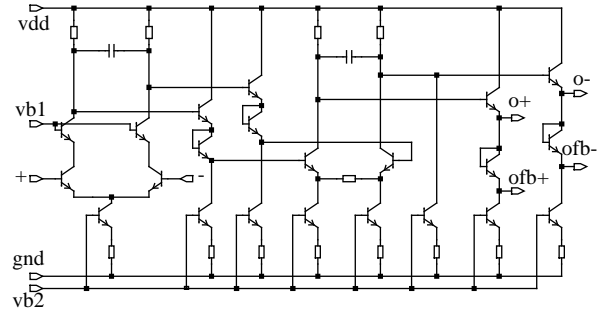


Fig. 2. Voltage amplifier of the preamplifier.

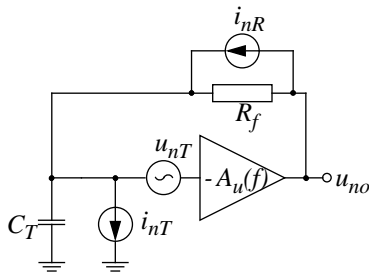


Fig. 3. Dominant noise sources of the preamplifier.

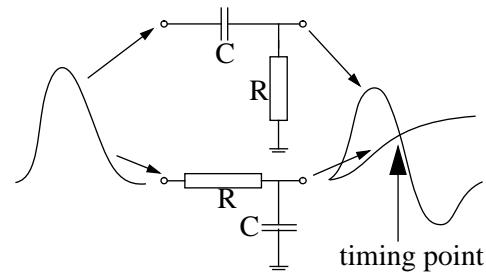


Fig. 4. Principle of the high/lowpass timing detector.

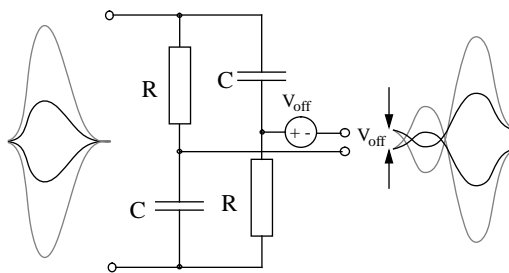


Fig. 5. Differential timing detector and walk error compensation.

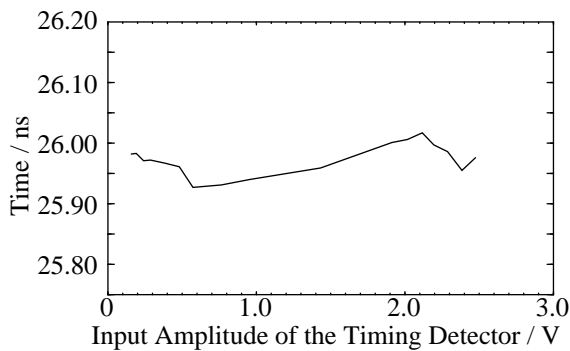
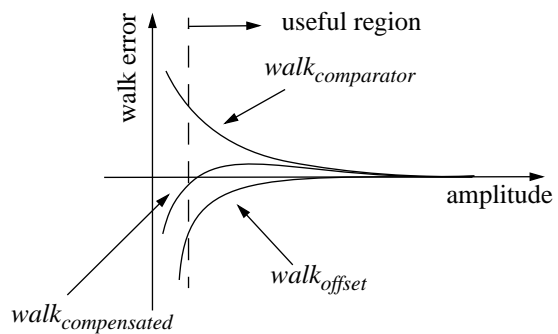


Fig. 6. Walk of the timing detector.

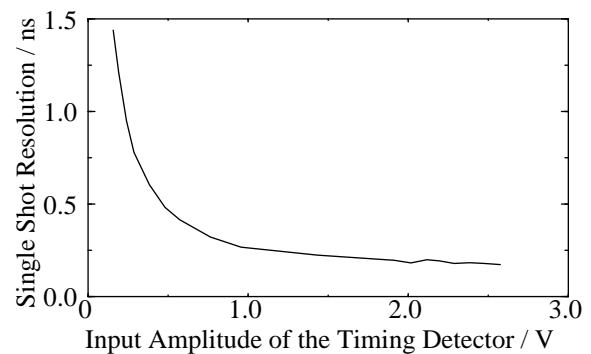


Fig. 7. Single-shot resolution of the timing detector.